SMC-TR-99-28

AEROSPACE REPORT NO.
TR-99(1494)-1

Graphite-Epoxy Motor Casing Health Monitoring System Demonstration

1 June 1999

Prepared by

J. V. OSBORN,[1] Y. C. CHAN,[1] C. M. KLIMCAK,[1] B. BROWN,[1]
B. WILLIAMS,[1] C. GUNN,[5] P. C. BRENNAN,[4] S. T. AMIMOTO,[2]
E. W. FOURNIER,[2] B. JADUSZLIWER,[1] D. C. MAYER,[1]
E. Y. ROBINSON,[3] D. VANDERKOI,[5] R. P. WELLE,[2]
and J. P. NOKES[2]

[1]Electronics Technology Center
[2]Mechanics and Materials Technology Center
[3]Center for Microtechnology
[4]Space Launch Operations
[5]SMC

Prepared for

SPACE AND MISSILE SYSTEMS CENTER
AIR FORCE MATERIEL COMMAND
2430 E. El Segundo Boulevard
Los Angeles Air Force Base, CA 90245

Space Systems Group

THE AEROSPACE CORPORATION
El Segundo, California

This report was submitted by The Aerospace Corporation, El Segundo, CA 90245-4691, under Contract No. F04701-93-C-0094 with the Space and Missile Systems Center, 2430 E. El Segundo Blvd., Los Angeles Air Force Base, CA 90245. It was reviewed and approved for The Aerospace Corporation by B. Jaduszliwer, Principal Director, Electronics Technology Center, and P. D. Fleischauer, Principal Director, Mechanics and Materials Technology Center. Lt Cary Gunn was the project officer for the program.

This report has been reviewed by the Public Affairs Office (PAS) and is releasable to the National Technical Information Service (NTIS). At NTIS, it will be available to the general public, including foreign nationals.

This technical report has been reviewed and is approved for publication. Publication of this report does not constitute Air Force approval of the report's findings or conclusions. It is published only for the exchange and stimulation of ideas.

Lt Cary Gunn, USAF
SMC/CLM

CAPT

REPORT DOCUMENTATION PAGE

Form Approved
OMB No. 0704-0188

1. AGENCY USE ONLY (*Leave blank*)	2. REPORT DATE	3. REPORT TYPE AND DATES COVERED
	1 June 1999	

4. TITLE AND SUBTITLE
Graphite-Epoxy Motor Casing Health Monitoring System Demonstration

5. FUNDING NUMBERS
F04701-93-C-0094

6. AUTHOR(S) J. V. Osborn, Y. C. Chan, C. M. Klimcak, B. Brown, B. Williams, C. Gunn, P. C. Brennan, S. T. Amimoto, E. W. Fournier, B. Jaduszliwer, D. C. Mayer, E. Y. Robinson, D. Vanderkoi, R. P. Welle, and J. P. Nokes

7. PERFORMING ORGANIZATION NAME(S) AND ADDRESS(ES)
The Aerospace Corporation
Technology Operations
El Segundo, CA 90245-4691

8. PERFORMING ORGANIZATION REPORT NUMBER
TR-99(1494)-1

9. SPONSORING/MONITORING AGENCY NAME(S) AND ADDRESS(ES)
Space and Missile Systems Center
Air Force Materiel Command
2430 E. El Segundo Boulevard
Los Angeles Air Force Base, CA 90245

10. SPONSORING/MONITORING AGENCY REPORT NUMBER
SMC-TR-99-28

11. SUPPLEMENTARY NOTES

12a. DISTRIBUTION/AVAILABILITY STATEMENT
Approved for public release; distribution unlimited

12b. DISTRIBUTION CODE

13. ABSTRACT (*Maximum 200 words*)

A prototype Multiparameter Sensor System is described for detection, localization, and magnitude determination of impacts as well as environmental condition monitoring of graphite epoxy composite structures. This system is applied to a test sample of a Delta-II solid rocket motor Graphite Epoxy Motor (GEM) casing. Impact detection and localization is performed with a Fiber Optic Bragg strain sensor, while 3-axis acceleration, temperature, pressure and humidity are sampled with Microelectromechanical (MEMS) sensors. All sensors are sampled with a National Instruments, Inc. data acquisition PCMCIA card, processed on a Pentium-II 200-MHz laptop. Sensor information is passed wirelessly to a remote user terminal for display and data storage. Acquisition and display software was written in LabView with custom codes developed for impact localization.

14. SUBJECT TERMS
Microelectromechanical sensors, MEMS, Multiparameter Sensor, Impact Detection, Delta-II, Health Monitoring, Graphite Epoxy Motor, Impact Monitor, Wireless Sensors, PCMCIA, LabView, graphite epoxy composite structures, condition based health monitoring

15. NUMBER OF PAGES
19

16. PRICE CODE

17. SECURITY CLASSIFICATION OF REPORT	18. SECURITY CLASSIFICATION OF THIS PAGE	19. SECURITY CLASSIFICATION OF ABSTRACT	20. LIMITATION OF ABSTRACT
UNCLASSIFIED	UNCLASSIFIED	UNCLASSIFIED	

Acknowledgments

The authors wish to thank the Aerospace Corporate Independent Research and Development Programs, the Air Force Delta System Program Office, and the Aerospace MLV Program Office for the support to carry out this FOS/MPS demonstration effort.

Contents

1. Introduction 1
2. Fiber-Optic Bragg Strain Sensor 3
3. MEMS Wireless Multiparameter Sensor 7
4. Combined GEM FOS/MPS Demonstration System 11
   - 4.1 Sensor and Sample Configuration 11
   - 4.2 MPS Data Acquisition and Impact Localization Computer 11
   - 4.3 MPS Remote Data Display Computer 12
5. Results 15
6. Conclusions 17

References 19

Figures

1. The effect of either tensile strain or increased temperature on the reflection spectrum of a Bragg grating 3
2. Conventional 4-wire resistive strain foil sensor verses fiber-optic strain sensor shown physically 4
3. Single Bragg sensor channel containing a 150-μW, ELED, 3 dB fiber-optic splitter, Bragg grating sensor, Bragg grating demodulator, and fiber-coupled InGaAs photodetector and variable gain preamplifier with tunable bandpass filtering 5
4. Dimensions of the composite panel and layout of the fiber optic sensors 5
5. MPS Communication network concept showing coverage of high-value assets through storage, transportation, and pre-launch operations 7
6. MPS signal acquisition and remote display block diagram showing the flow of information from the sensor front-end through the MPS data processor and wireless network to the remote user data display terminal 8

7. Multiparameter Sensor Package with 3-axis acceleration, temperature, pressure, and humidity sensors with interface to the fiber-optic sensor electronics outputs via BNC connectors 8

8. MPS sensor mounting adapter showing one single-axis MEMS accelerometer, one two-axis MEMS accelerometer, mounting block, and package interface to the GEM test article. 9

9. GEM MPS demo sensor (laptop computer not shown) and future palm-sized design of the multiparameter sensor. 10

10. Photo of the GEM test article, with four fiber sensors and MPS sensors attached 11

11. Data Acquisition Labview Display showing transient response of fiber sensors and X-Y plot of impact location on the 1.5 ft by 3 ft GEM sample panel 13

12. Remote User Labview Display showing impact location, relative impact magnitude, time sampled and peak accelerations for X,Y and Z-axis, temperature, humidity, and ambient atmospheric pressure. 13

Tables

1. MPS Sensor Performance Table 16

1. Introduction

Solid rocket Graphite Epoxy Motor (GEM) casings are susceptible to catastrophic damage due to blunt force impacts.[1] Following the explosion of Delta 241 (IIR-1) on January 17th, 1997, the failure investigation board concluded that the GEM casings should be inspected for damage just prior to launch. Subsequent investigations and feedback from industry have led to our proposal to instrument the entire fleet of GEMs from acceptance testing through erection on the launch pad with a continuous health monitoring system. This instrument would monitor and record adverse impacts, accelerations, strains, or environments that may cause damage to the GEM casings.

The key requirements for such surveillance of GEMs are an unobtrusive system that does not interfere with normal rocket motor operations, direct-wire and wireless flexibility, very long-term surveillance capability in stand-alone wireless mode, low power, and the ability to calibrate normal operational signatures vs. unusual serious events. Additionally, with a network of sensors on a large surface, it is possible to locate the area and magnitude where inadvertent impacts occur. A sensor with dc strain capability, such as the fiber-optic strain gage, can also witness excessive stress events that might be associated with incorrect handling operations, without any impact. Interest by the Medium Launch Vehicle (MLV) Program Office in the potential long-term application of such a system prompted the demonstration described in this report.

Technology developed in the Electronics Technology Center and the Mechanics and Materials Technology Center of The Aerospace Corporation under the Microelectromechanical Systems (MEMS) Corporate Research Initiative (CRI), Multiparameter Sensor (MPS) task and under Aerospace Corporate Independent Research and Development in Fiber-Optic Sensors is applied in the present demonstration.[2,3,4] These multi-year research programs have led, in this case, to the creation of a system concept that would allow the unobtrusive, continuous health monitoring of Graphite Epoxy Motor Casings and other impact-sensitive graphite epoxy structures. Our system concept uses a combination of fiber optic sensors and MEMS sensors organized in a distributive network such that both impact strains and environmental information can be detected, stored, and forwarded to a central computer.

The purpose of this laboratory demonstration was twofold: first, to verify that a distributed array of fiber-optic strain sensors could be used to determine both the position and relative magnitude of a mechanical impact on a laboratory-scale, graphite-epoxy composite panel; and second, to demonstrate that these sensors could be interfaced to a wireless, networked MEMS multiparameter environmental monitor measuring 3-axis acceleration, temperature, pressure, and humidity. This report describes the fiber-optic sensor suite and the multi-parameter sensor suite independently followed by a description of the combined GEM Fiber-Optic MPS (FOS/MPS) Health Monitoring System demonstrator.

2. Fiber-Optic Bragg Strain Sensor

The method for performing the task of impact localization relied on measurement of differences in arrival time between impulsive strain transients detected at different locations on the panel following an impact-induced elastic disturbance that propagated outward in all directions from the locus of impact. We used a spatially distributed array of fiber-optic Bragg grating sensors to detect these strain transients.

A fiber-optic Bragg grating sensor is a diffraction grating written by an ultraviolet laser technique in the core of single-mode fiber-optic waveguide.[5] It is a wavelength-selective passive optical element that reflects only a very narrow spectral band of light (FWHM ≈0.3 nm) whose peak wavelength is determined by the grating period. A typical Bragg grating reflection spectrum is shown by the solid line in Figure 1. The grating period can be modified by both stress-induced strain and by temperature, resulting in a shift in the wavelength of light reflected by the sensor. The dotted line in Figure 1 depicts the effects of either tensile strain or increased temperature on the reflection spectrum of the sensor. In both cases, it shifts to a longer wavelength. The relationships between peak sensor wavelength and the local strain and temperature are indicated in Figure 1. Those quantities can be determined from a measurement of the fractional Bragg wavelength shift. Numerous demultiplexing techniques have been developed for use with spatially distributed arrays of Bragg grating sensors, and effective methods for differentiating between the effects of temperature and strain have also been devised.[6]

Bragg sensors possess many advantages. They are lightweight and non-intrusive, they can be multiplexed to provide the high sensor density required for smart structures and materials, they directly encode strain and temperature into wavelength, they are immune to electromagnetic interference, and the sensing elements are all optical thus permitting operation in electrically sensitive environments.[7]

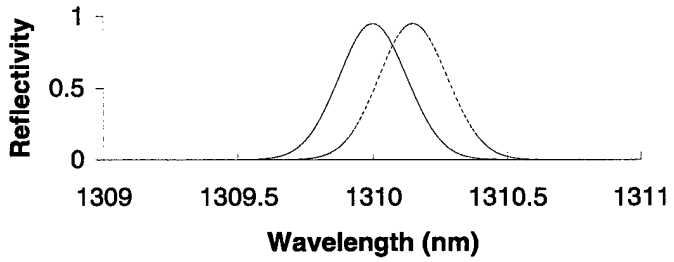

At 1310 nm, $\Delta\lambda = 0.001$ nm/με, $\Delta\lambda = 0.00874$ nm/°C

Figure 1. The effect of either tensile strain or increased temperature on the reflection spectrum of a Bragg grating.

If desired they could even be embedded directly into a filament-wound composite during its manufacture.[8] Additionally, fiber-optic sensors are smaller than conventional strain sensors and require no wire cabling to the sensor (Figure 2). These features make them ideally suited for use in a distributed GEM impact monitoring system. Both static and dynamic effects could potentially be observed. However, a determination of the magnitude and location of a mechanical impact, the ultimate goal of this demonstration, can be made solely from measurements of the arrival time and peak amplitude of the fast, transient strain impulse. Therefore, electronic filtering of the sensor response could be implemented in order to reject all static and transient signals outside a selected bandpass. This filtering procedure was employed in this work because it eliminated all effects of statically imposed strain, as well as slow fluctuations and drift in room temperature.

A complete Bragg sensor channel is shown in Figure 3. Each channel had its own querying light source, which was a 150-μW, continuously operating, edge-emitting light-emitting diode (ELED) with a peak wavelength of 1310 nm, a standard 3 dB fiber-optic splitter for coupling light to and from the sensor, a Bragg sensor mounted on the composite test article, a narrowband demodulator that converted the strain-induced wavelength shift into an intensity change, and its own fiber-coupled InGaAs photodetector and variable gain preamplifier with tunable bandpass filtering. The 3dB roll-off points of the high- and low-pass filters were adjusted to 30 Hz and 3 kHz, respectively.

A wavelength-to-intensity sensor demodulation technique was selected because it is both the simplest and most economical method for determining the Bragg wavelength shift. The demodulator was also a Bragg grating having a similar spectral bandwidth but with a peak wavelength that was shifted to shorter wavelength by one-half of a bandwidth relative to that of the Bragg sensor on the composite test article. This shift optimized the performance of the analyzer, and it ensured the largest possible linear operating region.

The location and configuration of the fiber sensors for this demonstration are shown in Figure 4. One of the sensors was bonded using gap-filling, catalyst-activated polycyanoacrylate cement. The other three sensors were mounted onto the surface with standard electrical tape. While the use of tape may have affected the magnitude of the observed strain transients, it did not alter their arrival times; we believe that the tape had little or no effect on our determination of impact location. To expedite assembly of the laboratory demonstration, we built four separate and parallel Bragg strain sensor channels rather than use a single serial channel. This simplified our task and permitted maximum flexibility in designing the system because sensor demultiplexing was not necessary. However, a GEM monitoring system could be constructed with serial, parallel, or even a combined sensor deployment topology.

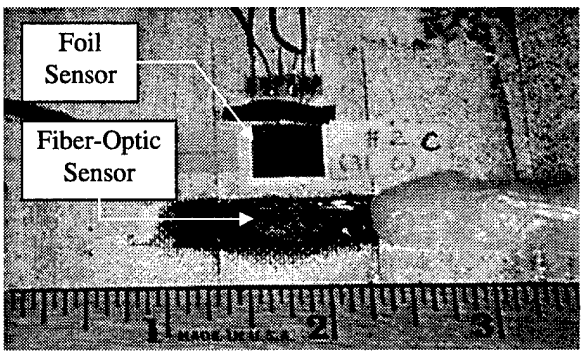

Figure 2. Conventional 4-wire resistive strain foil sensor verses fiber-optic strain sensor shown physically. The actual 100-μm-diam by 1-cm long fiber sensing element is difficult to see in this figure; most of what is seen here is the area that has been cleaned by light sanding to directly bond the fiber sensor to the test article.

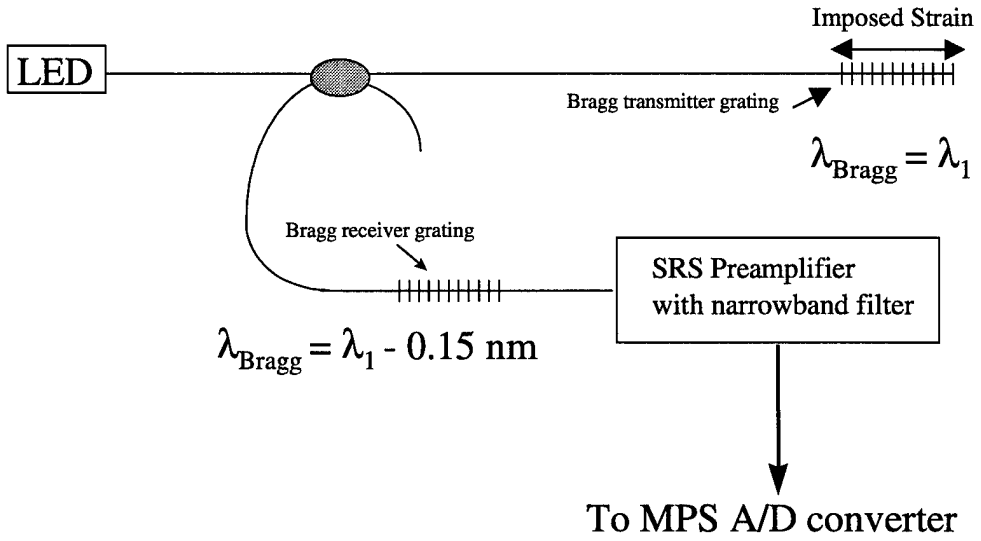

Figure 3. Single Bragg sensor channel containing a 150-μW, ELED, 3 dB fiber-optic splitter, Bragg grating sensor, Bragg grating demodulator, and fiber-coupled InGaAs photodetector and variable gain preamplifier with tunable bandpass filtering.

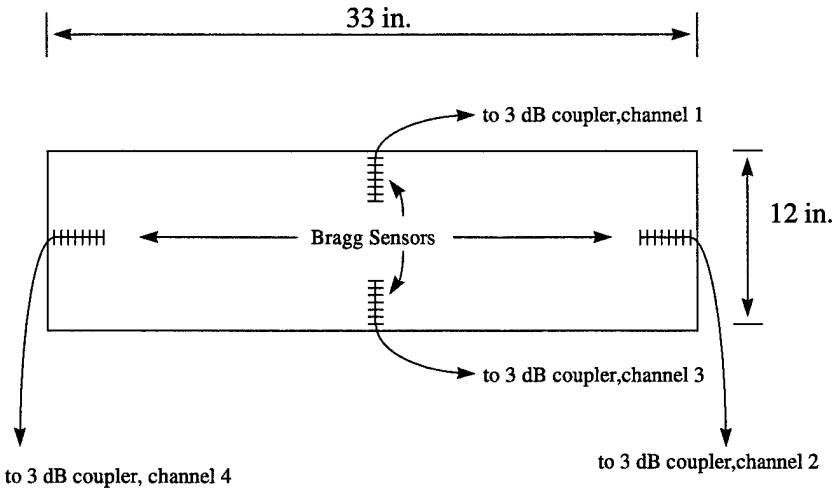

(Bragg sensors not to scale, actual length = 1 cm)

Figure 4. Dimensions of the composite panel and layout of the fiber optic sensors.

The resultant fiber-optic transient output signals from each sensor channel were acquired and digitized in the MPS system. Four of these channels provided data input to the MPS laptop PC running Labview virtual instrumentation software where impact localization and relative impact magnitude were determined.

3. MEMS Wireless Multiparameter Sensor

A MEMS Wireless Multiparameter Sensor (MPS) is a combination of multiple microelectromechanical sensors measuring different environmental parameters integrated together with local computing, data storage, wireless communication, and power. The MPS is organized in a network such that hundreds of such nodes may communicate to a centralized data-archiving computer (Figure 5). The need for such a sensor network is not limited to GEM health monitoring. The MPS system may be employed wherever high-value assets are stored, transported, or handled, and where the past history of shock, strain, temperature, humidity, or pressure is of concern to the operation or reliability of that high-value asset.

The present implementation of the Multi-Parameter Sensor (MPS) electronic hardware leverages off of commercially available technology to provide sensor data acquisition and processing, local memory storage, and networked RF communications. The design of the MPS is partitioned into an MPS sensor box and an MPS processor unit, as shown in Figure 6. The partitioned design allows for customized arrangements of sensors to be tailored to a specific measurement, as well as to provide a common data collection, processing, storage, and communication infrastructure.

The primary goal of the MPS aspect of this demonstration was the development of a networked, wireless, MPS demonstration system capable of collecting and processing strain, 3-axis acceleration, temperature, humidity, and pressure data from a combination of fiber-optic and MEMS sensor

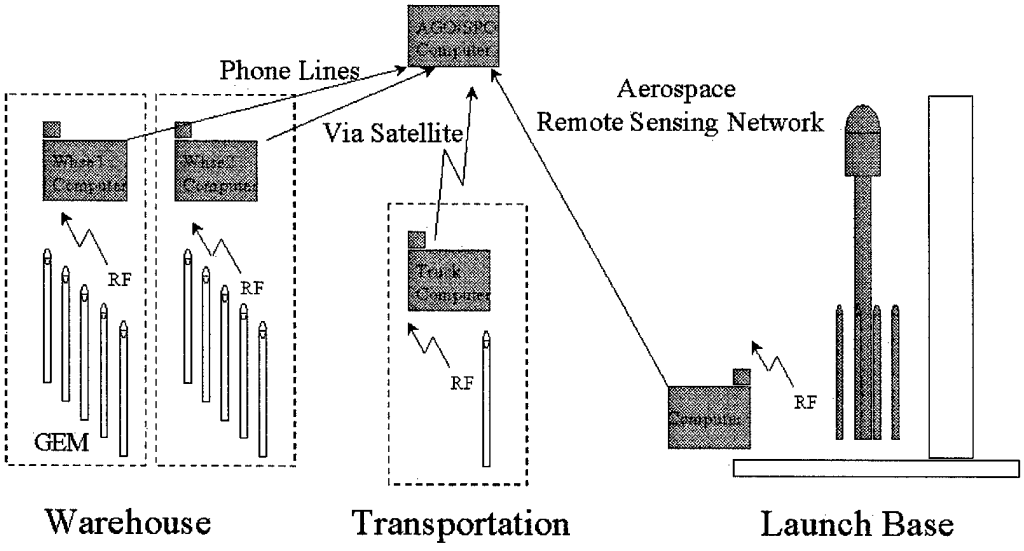

Figure 5. MPS Communication network concept showing coverage of high-value assets through storage, transportation, and pre-launch operations.

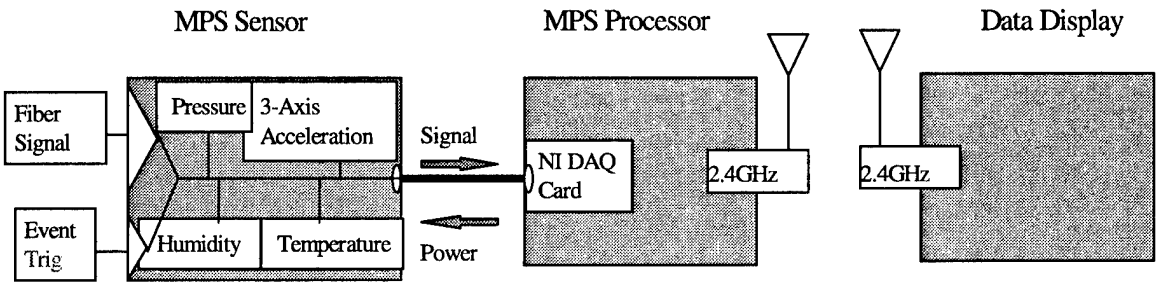

Figure 6. MPS signal acquisition and remote display block diagram showing the flow of information from the sensor front-end through the MPS data processor and wireless network to the remote user data display terminal. Up to 50 MPS nodes can be supported.

sources. This system can be scaled up such that up to 50 local MPS sensor collection sites can forward their data, using a wireless network, to a local data collection hub for data archiving or user display.

In this demonstration a 2 x 2 x 4 in. metal box, shown in Figure 7, housed the MPS environmental sensors in addition to a 3-axis accelerometer sensor. The environmental sensing package consisted of the Ohmic HC-700 humidity sensor, the Motorola MPX5100A pressure sensor, and the Analog Devices AD592 temperature sensor. The sensor package was rigidly fastened to the top of the box, and holes were drilled to provide the sensors with exposure to the ambient environment.

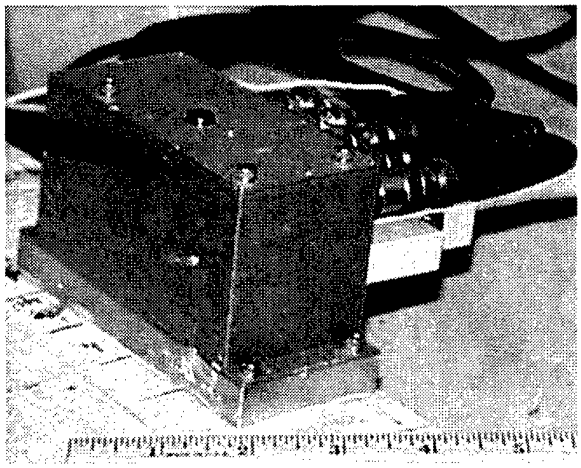

Figure 7. Multiparameter Sensor Package with 3-axis acceleration, temperature, pressure, and humidity sensors with interface to the fiber-optic sensor electronics outputs via BNC connectors.

The dynamic sensing package housed within the sensor box was a three-dimensional accelerometer system consisting of one Analog Devices ADXL150 and one ADXL250 accelerometer. To accurately capture the dynamic response of the test structure, it was necessary to decouple the acceleration response of the test structure from the acceleration response of the sensing package. System requirements, in general, prevent the accelerometers from being mounted directly to the test article. Our solution, in this case, was to provide a rigid path with known material characteristics between the sensors and the test article. The vibrational conduit connecting the sensor packaging to the test structure consists of a solid aluminum test package mount and an aluminum accelerometer mounting block (Figure 8).

When assembled, the sensors were attached to adjacent sides of the accelerometer mounting block using a thin layer of epoxy. The mounting block was then rigidly fastened to the test package mount by two cap screws. The current GEM demonstrator incorporated a thin layer of epoxy as the fastener connecting the test package mount to the test article.

In addition to the environmental and dynamic sensing packages, the complete sensor assembly contained five mini-BNC connectors that served as input ports for the trigger and optical signals used by the fiber-optic system. The combined signals were channeled through a National Instruments 68-pin shielded cable to the MPS data acquisition laptop computer. Power for the MEMS sensors was provided by the laptop computer, while power for the fiber-optic drive electronics was independently provided.

To reduce cost and effectively perform the GEM FOS/MPS demonstration with the most flexibility, we chose to implement the MPS data acquisition portion of the effort with a conventional COTS laptop computer and wireless LAN. As part of the MEMS CRI effort, we are developing custom

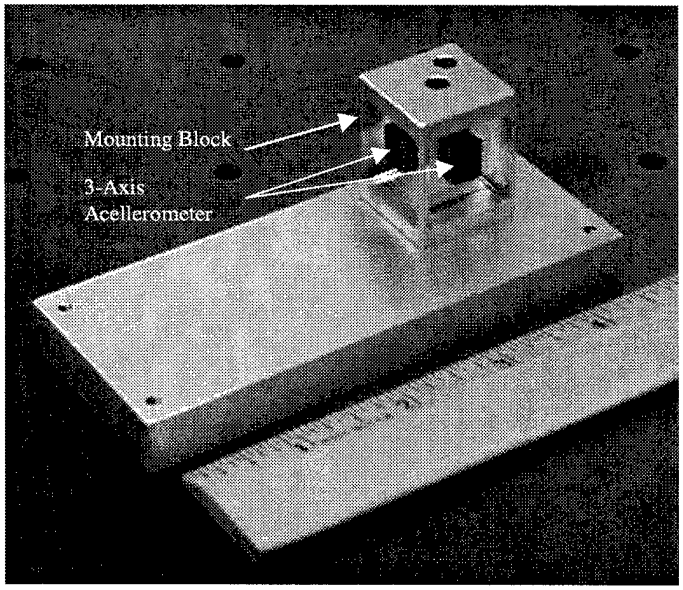

Figure 8. MPS sensor mounting adapter showing one single-axis MEMS accelerometer, one two-axis MEMS accelerometer, mounting block, and package interface to the GEM test article.

palm-sized MPS hardware (Figure 9). This future version of the MPS will have 3-axis acceleration, temperature, pressure, and humidity sensors, a microcomputer, event storage memory, time keeping, wireless communication, and power integrated into one miniaturized package.

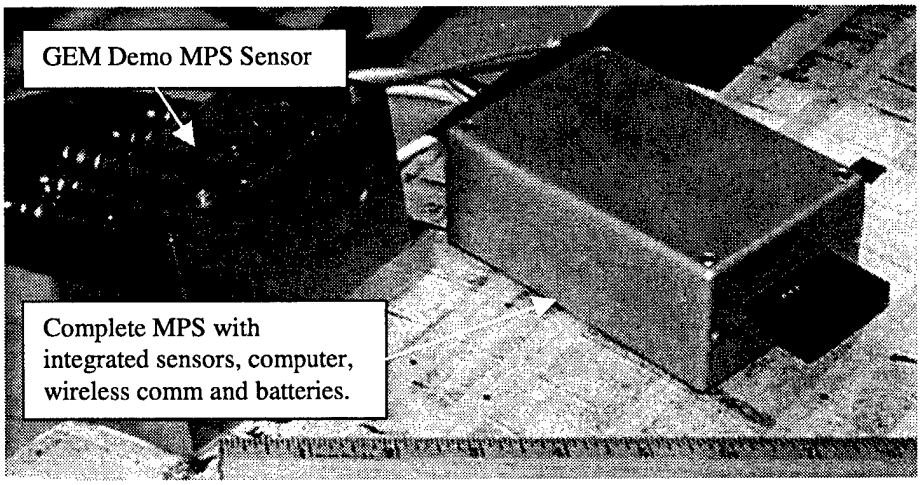

Figure 9. GEM MPS demo sensor (laptop computer not shown) and future palm-sized design of the multiparameter sensor.

4. Combined GEM FOS/MPS Demonstration System

Initially, the Fiber-Optic Strain (FOS) sensor and MPS systems were made to function independently. When operating separately, the FOS read-out electronics were interfaced to a stand-alone computer for data collection and position determination, while the MPS system collected multi-parameter environments data, and processed, wirelessly transmitted, and displayed MPS information to a remote user display laptop. Following successful independent operation on the GEM test article, the two systems were merged both in terms of data acquisition hardware and in data processing software. The merged systems became the GEM Fiber-Optic Strain and Multiparameter Sensor (FOS/MPS) health monitoring demonstrator.

4.1 Sensor and Sample Configuration

The fiber optic impact monitoring system was constructed with four Bragg grating sensors that were mounted on the cleaned outer surface of a rectangular composite panel (≈1 ft x 3 ft) provided by Dr. Jim Nokes of MMTC. The output of the FOS signal processing electronics was then input to the MPS sensor box and routed to the data acquisition computer (Figure 10). This particular GEM specimen was a section of an actual Delta II motor casing that was recovered from a hydroburst test. It was not attached to inert fuel, but approximately a one-half-inch thickness of elastomeric thermal shielding material was still bonded to its inner surface.

4.2 MPS Data Acquisition and Impact Localization Computer

A Hitachi VisionBook Plus 5000 with a National Instruments E-Series Data Acquisition Card processed the incoming analog sensor signals. The data sampling function of the FOS/MPS is provided by a commercially available 16-channel National Instruments DAQ PCMCIA card (AI-16XE-50)

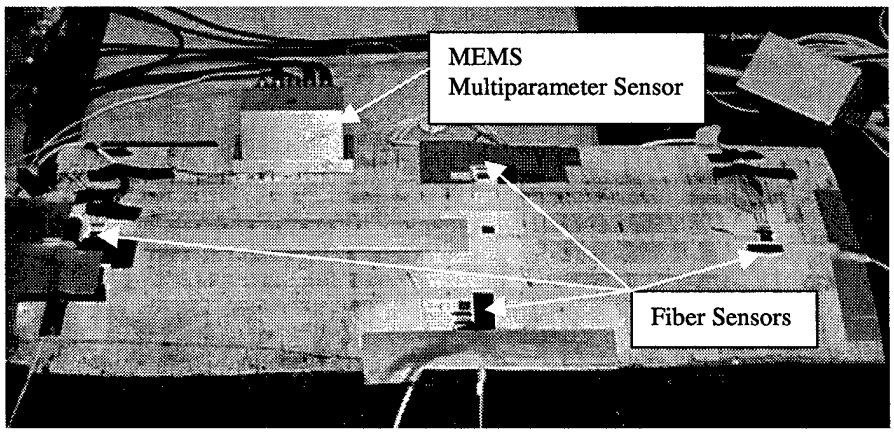

Figure 10. Photo of the GEM test article, with four fiber sensors and MPS sensors attached. In addition to the sensor suite, two laptop computers (not shown) are needed to collect and remotely display impact data.

having 16-bit resolution. This card was configured for eight differential input bipolar channels sampled at 25 ksample/s for FOS data collection, while three additional channels were used at a 500-Hz collection rates for the non-time-sensitive MPS measurements. The software running the overall data acquisition process was Labview 5.0.

Two separate event triggering and position determination methods were incorporated into the system to determine impact location. Initially, an external trigger from an impact hammer equipped with an internal impulse-measuring accelerometer was used to trigger data acquisition. After a sample set was collected, a Fortran program computed the differences in the transient arrival time between pairs of fiber sensors (Δt_{ij}) from the zero crossings of their transient signals. The program then compared this measured set of arrival time differences to a stored table of expected arrival time differences calculated from prior measurements of the propagation speed of the disturbance and the distances between the sensor locations and a dense grid of potential impact points. The coordinates of the stored set that exhibited the smallest deviation from the measured set established the impact site.

Later in an alternate preferred method, we relied on the impact transient itself to trigger the location determination algorithm. In this case, the algorithm used to determine impact location was based on a modified two-dimensional Hooke-Jeeves numerical search. Once a sensor event had been detected, the search routine began its search for the point of impact by picking an arbitrary initial starting point between the four fiber sensors. Once the point was chosen, the program determined the distance from the starting point to each of the four sensors. Next, the distances were compared to the time values provided by the fiber-optic sensors. The degree to which the distances and times match was assessed, and a numerical merit based upon the similarity between the ratios was assigned to the initial starting point. Numerical merits were calculated in the same manner for points surrounding the initial starting point until an optimal merit was discovered. The position with the optimum merit corresponded to the actual impact location.

In both cases, the relative magnitude of the impact was derived from the peak intensity of the transient signal that originated from the sensor closest to the predicted impact site. This peak intensity was multiplied by the distance between the sensor and the impact site to normalize for the expected 1/R decline of signal amplitude with distance. Once calculated, the impact location and relative magnitude information was immediately displayed on the data acquisition computer (Figure 11). Following this, the information was joined with the MPS environmental data, and an event data file was written from the acquisition computer to the hard drive of the remote display computer via the wireless network.

4.3 MPS Remote Data Display Computer

An important part of the demonstration was the wireless data exchange. A second Hitachi Laptop using a wireless local area network (LAN) served as the display computer. The hard drives of the two computers were cross-linked via the wireless network with both having shared file access. The remote computer also used Labview software to access files and plot FOS and MPS data. The combined FOS/MPS user screen displayed the X-Y impact location, relative magnitude, three-axis acceleration, pressure, temperature, and humidity measurements. As each new information packet was stored on the remote display hard drive, the graphs and gauges of the FOS/MPS display were updated (Figure 12).

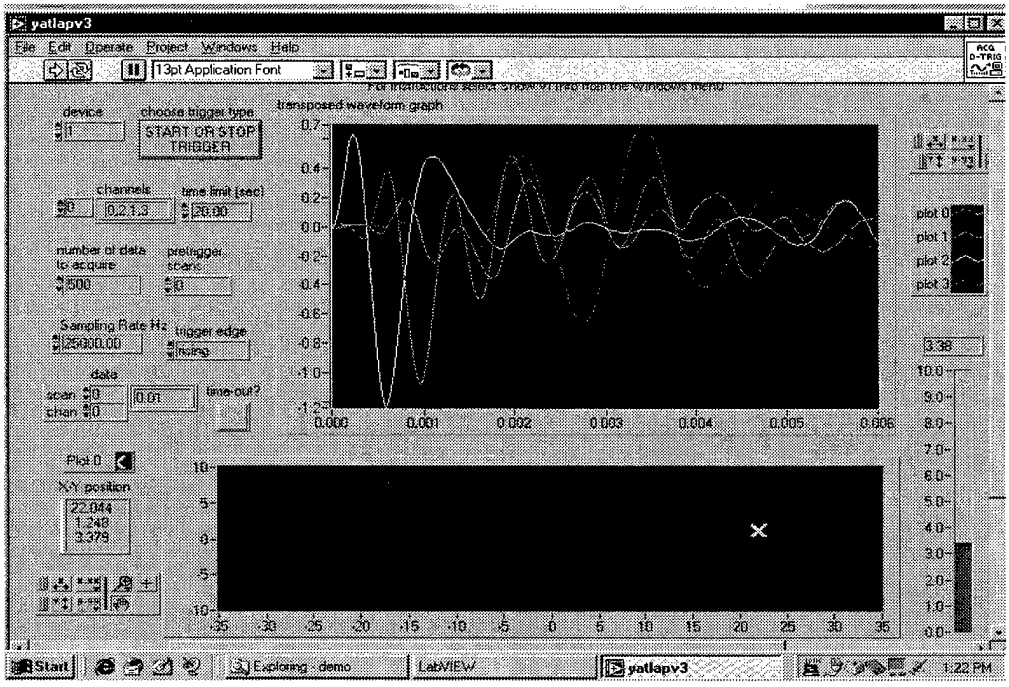

Figure 11. Data Acquisition Labview Display showing transient response of fiber sensors (top) and X-Y plot of impact location on the 1.5 ft by 3 ft GEM sample panel (bottom). "X" marks the location of impact on the sample panel in this display. Relative magnitude is shown with a vertical bar graph (lower right).

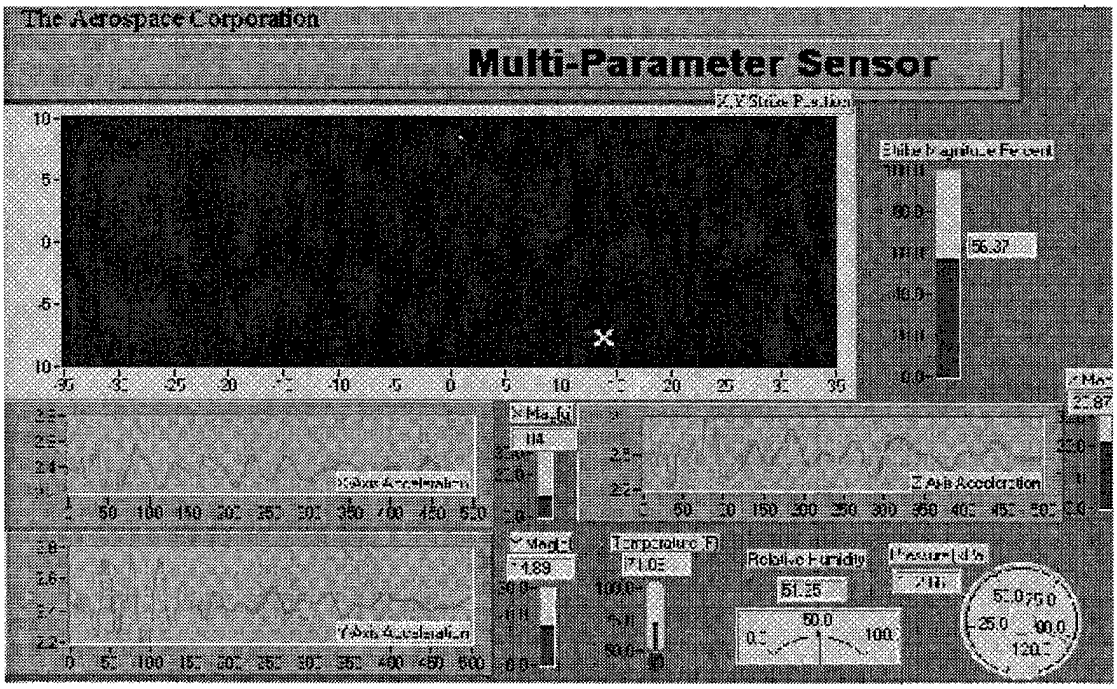

Figure 12. Remote User Labview Display showing (From Top to Bottom) impact location, relative impact magnitude, time sampled and peak accelerations for X,Y and Z-axis, temperature, humidity, and ambient atmospheric pressure.

5. Results

A hard-copy printout of the data acquisition Labview display screen immediately following an impact is shown in Figure 11. The figure at the upper right, labeled with the heading "transposed waveform graph," shows the filtered and amplified output of each of the four fiber sensor channels. These four signals provide all the information required to determine the impact location and relative magnitude. The rectangular region below these signals represents an image of the composite panel. The X on this panel designates the computed impact site. To the right is a vertical bar graph that indicates the relative magnitude of the impact on a scale from 0 to 10. This Labview display indicates that this particular impact occurred at (x,y) coordinates (22,1) with a magnitude of 3.3. (Note: The coordinate dimensions are in centimeters). Repeated impacts at this same location produced an uncertainty in impact location of approximately ± 2 cm. Impacts at other sites (with the exceptions noted below) also yielded this uncertainty. The uncertainty in the computed impact magnitude was not determined.

The image of the panel reproduced in the Labview display is 7.9 in x 27.6 in, while the actual panel is 12 in x 33 in. The excluded area lies near the boundary of the panel, a region where effects due to the boundary itself may interfere with elastic wave propagation. For example, boundary reflections may contribute appreciably to the transient response of the sensor, distorting the first observed impulse for impacts that occur close to the boundary. We did observe indications of these reflections and their distorting effects in some transient responses. In this case, the location algorithm would not accurately determine the impact location. In fact, our predicted locations of impacts near the boundary were often inaccurate, and we believe this error to have been caused by boundary effects.

Additionally, there was approximately a 5-cm-radius circular region centered at the coordinates (-25, -5) where impact locations could not be determined. Impacting within this circle produced sound that differed greatly in pitch and acoustic quality from that produced by impact at other locations. We believe this region contained a defect or delamination, perhaps generated during the hydroburst of the composite case from which we obtained the panel. Our earlier propagation speed measurements in this region indicated a reduced speed, consistent with a loss of mechanical integrity at this location.

Multiparameter environmental sensor data was derived from commercial MEMS and conventional sensors. MPS sensor performance data is shown in Table 1. In this demonstration, MPS data was sampled, averaged, and stored at the time of impact; however, it is expected that in actual use, the environmental portion of the data stream would be continuously logged at a low rate to detect exceedances during storage or transportation. All FOS and MPS data were wirelessly transmitted to a roving remote laptop computer that displayed the impact location, its relative magnitude, and data from the multiparameter sensor suite (temperature, pressure, humidity, and 3-axis acceleration) as shown in Figure 12.

Table 1. MPS Sensor Performance Table

Sensor Type	Model	Data Range	Power Requirements
Temperature	Analog Devices AD592	–25°C to +105°C, ±0.8°C	4–30 VDC, 120 μA
Pressure	Motorola MPX5100A	15–115 kPa, ±3 kPa	4.75–5.25 VDC, 5–10 mA
Humidity	Ohmic HC-700	0–100% RH, ±2% RH	4–9VDC, 0.2 to 2.0 mA
1-Axis Acceleration	Analog Devices ADXL150	±50 g	4.75–5.25 VDC, 1.8 mA
2-Axis Acceleration	Analog Devices ADXL250	±50 g	4.75–5.25 VDC, 3.6 mA

A qualitative experiment was also executed to determine the approximate range of the two wireless network PCMCIA cards. Outdoors, away from any interfering buildings, the two laptop computers demonstrated communication rates of 537 kb/s at a separation of 800 ft. At a distance of less than 40 ft, the devices transferred information at rates in excess of 1.5 Mb/s. The optimum direction of the antennas was determined to be in the plane of the laptop keyboard, away from the operator. As part of the GEM FOS/MPS demonstration, the remote user data display computer was taken outdoors, and the sensor node communicated without disruption through a separating cinder block wall. It is presumed that indoor environments could produce multipath interference and potentially reduce the antennas' effectiveness.

One technical issue identified during the testing was determined to be an anisotropy in the response to incident stress waves on the surface of the GEM sample. The wave shape created by a stress wave disturbance was not only a function of the magnitude of the disturbance but also the angle of incidence to the sensor. Consequently, the sensor response produced by a 5-lb impact 3 in. away tangential to the sensor was not identical to the same impact 3 in. longitudinally from the sensor. This effect complicated signal processing and degraded the reliability of the location determination algorithm. Further refinement of the sensor signal processing algorithm will reduce this to a negligible effect.

6. Conclusions

With this demonstration, we have shown that it is possible to develop an unobtrusive system that uses a network of fiber-optic sensors on a GEM surface to detect and locate the area and magnitude where inadvertent impacts occur. Additionally we have interfaced this impact sensor to a wireless MEMS Multi-Paramter Sensor system to make a coordinated impact load and storage environments measurement. This information can then be used to determine whether impacts or environmental conditions have occurred to affect the structural integrity of the graphite-epoxy structure.

Our system may also be calibrated with small impacts from an instrumented tap-hammer that measures the **F-t** impulse delivered to the structure to permit an absolute measurement of impact magnitude. Additionally, we found that the fiber-optic sensor may be used in a dc strain mode; operated in this manner, the sensor can also witness excessive stress events that might be associated with incorrect handling operations without an impact.

While this demonstration only employed a relatively small lab-scale test article, the system developed here could be scaled up to permit development of an effective impact monitoring system for the Delta GEMs. The requirements and specifications for such a system will require an investigation of the impact behavior and mechanical characteristics of the GEM in greater detail. Preliminary experiments conducted in January 1998 on a full-scale inert motor at Cape Canaveral have indicated that impacts can be detected as distant as 15 ft from a fiber-optic Bragg grating sensor. This preliminary full-scale field data, together with the present laboratory FOS/MPS impact demonstration, establishes the feasibility of developing a successful Delta GEM health monitoring system.

References

1. "Delta II GEM, K522 Case Impact and Hydro/Structural Test Final Report," The Boeing Corporation, August 27, 1997, Contract F04701-93-C-0004, P00049, CDRL A004.

2. S. T. Amimoto, R. Crespo, E. W. Fournier, J. V. Osborn, H. Ozisik, B. H. Weiller, E. M. Yohnsee, "Development of Launch Vehicle Nanotechnology Instrumentation at The Aerospace Corporation," *Proceedings of the 44th International Instrumentation Symposium*, Aerospace Industries Division of ISA, Reno, NV, May 4–7, (1998)

3. S. T. Amimoto, R. Crespo, E. W. Fournier, J. V. Osborn, H. Ozisik, B. H. Weiller, E. M. Yohnsee, "Atlas Payload Transporter Vibration and Acceleration Characterization Using MEMS Sensors at Vandenberg AFB," TOR-98(8260-01), The Aerospace Corporation (1998).

4. Sherwin Amimoto, Brett Brown, Eric Fournier, Jon Osborn, Bruce Weiller, Brice Williams and Ernest Yohnsee "Sensor Node Development of a Low Power, High Data Rate Multi-Parameter Sensor (MPS) System," Space Technology and Applications International Form-1999, Albuquerque, NM.

5. W. W. Morey, G. Meltz, and W. H. Glenn, "Fiber Bragg grating sensors," *Proc. SPIE Fiber Optic & Laser Sensors VII*, **1169**, p. 98 (1989).

6. A. D. Kersey, M. A. Davis, T. A. Berkoff, D. G. Bellmore, K. P. Koo, and R. T. Jones, "Progress Towards the Development of Practical Fiber Bragg Grating Instrumentation Systems," *Proc SPIE,* **2839**, p. 40 (1989).

7. Alan D. Kersey, Michael A. Davis, Heather J. Patrick, Michel LeBlanc, K. P. Koo, C. G. Askins, M. A. Putnam, and E. Joseph Friebele, "Fiber Grating Sensors," *J. Lightwave Technology*, **15**, p. 1442 (1997).

8. *Fiber Optic Smart Structures*, edited by Eric Udd, John Wiley & Sons Inc., New York (1995).